

Placenta-derived factors contribute to human iPSC-liver organoid growth

Received: 8 November 2023

Accepted: 25 February 2025

Published online: 13 March 2025



Yoshiki Kuse^{1,2}, Shinya Matsumoto¹, Syusaku Tsuzuki¹, Erica Carolina^{1,3}, Takashi Okumura¹, Toshiharu Kasai¹, Soichiro Yamabe^{1,3}, Kiyoshi Yamaguchi⁴, Yoichi Furukawa⁴, Tomomi Tadokoro⁵, Yasuharu Ueno¹, Takayoshi Oba¹, Naoki Tanimizu¹ & Hideki Taniguchi^{1,5}✉

Organoids derived from human induced pluripotent stem cells (hiPSC) are potentially applicable for regenerative medicine. However, the applications have been hampered by limited organoid size and function as a consequence of a lack of progenitor expansion. Here, we report the recapitulation of progenitor expansion in hiPSC-liver organoids based on the analysis of mouse development. Visualization of blood perfusion and oxygen levels in mouse embryos reveals a transient hypoxic environment during hepatoblast expansion, despite active blood flow. During this specific stage, the placenta expresses various growth factors. Human and mouse placenta-liver interaction analysis identifies various placenta-derived factors. Among them, IL1 α efficiently induces the growth in hiPSC-liver organoids as well as mouse fetal livers following progenitor expansion under hypoxia. Furthermore, subsequent oxygenation demonstrates that progenitors expanded by IL1 α contribute to hiPSC-liver organoid size and function. Taken together, we demonstrate that treatment with the placenta-derived factor under hypoxia is a crucial human organoid culture technique that efficiently induces progenitor expansion.

Organoid derived from human induced pluripotent stem cells (hiPSC) have tissue-like structures and exhibit various organ-specific functions through the multiple cell communications^{1–3}. Therefore, hiPSC-organoids allow us to recapitulate the aspects of human diseases as well as development, and they could be potentially applicable for regenerative medicine^{4,5}. However, their application has been hampered by limited their size, function, and long-term maintenance. Robust expansion of progenitors is crucial for increasing organ size and generating functional cells during development^{6,7}, leading to the generation of a progenitor pool in adults. Until now, there is growing body of evidence for the existence of progenitor pool within some adult organs, which often functions to maintain organ function and homeostasis after injury^{8–11}. Therefore, the induction of progenitor expansion in hiPSC-organoid could recapitulate in vivo organ growth

and homeostasis, although the key regulators of the progenitor expansion are currently unknown.

Organs typically receive nutrients and oxygen through blood perfusion. Fetal growth restriction occurring at a rate of ~8–10% is due to inadequate blood circulation in the organs, which is associated with tissue damage¹². Placental dysplasia has been linked to impaired fetal growth in organs like the liver and pancreas^{13,14}. Maternal nutrient restrictions and impaired placental function can result in decreased liver size¹⁵. The secretion of endocrine factors such as insulin-like growth factor 1 (IGF1) also plays a key role in the growth of organs, with a recent study demonstrating that placenta-derived endocrine factors such as superoxide dismutase 3 (SOD3) contributed to the development of metabolic functions of the liver in the offspring^{16,17}. In addition, loss of placental *Igf2* impairs the hepatic function¹⁸. These evidences

¹Division of Regenerative Medicine, The Institute of Medical Science, The University of Tokyo, Tokyo, Japan. ²Molecular Pharmacology, Department of Biofunctional Evaluation, Gifu Pharmaceutical University, Gifu, Japan. ³Graduate School of Frontier Sciences, Computational Biology and Medical Science, Kashiwa, Japan. ⁴Division of Clinical Genome Research, The Institute of Medical Science, The University of Tokyo, Tokyo, Japan. ⁵Department of Regenerative Medicine, Yokohama City University Graduate School of Medicine, Kanagawa, Japan. ✉e-mail: rtanigu@g.ecc.u-tokyo.ac.jp

suggested that the liver, being the first organ to receive blood from the placenta, heavily relies on placenta-derived blood for normal growth. However, there is limited evidence on placenta-fetal organ interactions and the specific placenta-derived endocrine factors that drive organogenesis.

Here, we revealed that placenta-liver interaction occurs under a transient hypoxic environment and contributes to hepatoblast (i.e., liver progenitor) expansion. At this specific stage, the placenta expresses various factors, including interleukin 1 alpha (IL1 α), which induce hepatoblast expansion in hiPSC-liver organoids as well as mouse fetal livers under hypoxia. Collectively, this study demonstrated that the recapitulation of transient placenta-liver interaction promotes the hiPSC-progenitor expansion and organoid growth.

Results

Determination of the stages of initial blood perfusion into the liver

The impact of physiological blood perfusion on liver growth remains unknown, although the influence of retroperfusion derived from the heart is partly assessed¹⁹. The relationship between physiological blood perfusion and liver growth was evaluated by visualizing placenta-derived blood perfusion of mouse embryos. AlexaFluor647 (i.e., fluorescent probe)-conjugated-lectin and anti-CD31 antibody were injected through the umbilical vein (Fig. 1A) with macroscopic evaluation revealing that the former primarily stained blood cells rather than endothelial cells while the latter specifically labeled blood vessels in the fetus (Supplementary Fig. 1A and Fig. 1B). Histological analysis showed that anti-CD31 antibodies labeled the perfused blood vessels in the liver, specifically in the region indicated by HNF4 α ⁺ hepatoblasts (i.e., liver progenitors) (Fig. 1C).

Anti-CD31 antibody perfusion method was then combined with whole-mount immunostaining to allow evaluation of the onset of blood perfusion into the liver. Perfused CD31⁺ blood vessels within the liver between E9.5 and E11.5 were observed under confocal microscopy after tissue clearing. The area of HNF4 α ⁺ hepatoblasts was selected as the region of interest to visualize the 3D image using Imaris software²⁰ (Fig. 1C and Supplementary Fig. 1B). The perfused blood vessels could be observed at E10.5 and E11.5 but not E9.5 (Fig. 1D), suggesting that placenta-derived blood perfusion into the liver commenced at E10.5.

Then, we investigated the contribution of placenta-derived blood to liver growth by preventing blood flow to the liver through ligation of the maternal uterine artery at E9.5 and E10.5. The fetal mice were collected 6 h after ligation (Supplementary Fig. 2A), and the findings indicated that ligation at E10.5 (but not E9.5) led to a remarkable decrease in liver and vascular volume when compared to the control group (Supplementary Fig. 2B–E). The decrease in the number of Ki67⁺ cells in the liver upon ligation at E10.5 suggested that placenta-derived blood perfusion influenced the proliferative capacity of fetal liver cells, resulting in an increase in liver size (Supplementary Fig. 1F). These findings suggest that the increase in liver size relied on placenta-derived blood perfusion at E10.5.

Localized blood perfusion at E10.5 promotes the growth of the ventral liver lobes

The 3D analysis revealed uneven blood perfusion into the liver at E10.5 (Fig. 1D), with perfused vessels primarily concentrated in the ventral lobes over the dorsal lobes. Visualization and quantification of perfused CD31⁺ blood vessels in the ventral and dorsal lobes showed abundant CD31⁺ perfused areas in the ventral lobes compared to the dorsal lobes at E10.5, indicating that placenta-derived blood predominantly perfused the ventral part of the liver at this stage (Fig. 1E, F). However, the CD31⁺ perfused areas were similar in the ventral and dorsal lobes of the liver at E11.5 (Fig. 1E–G). The size of the dorsal and ventral lobes was not significantly different at E10.5, but the ventral lobes were significantly larger than the dorsal lobes at E11.5 (Fig. 1E, H). Furthermore, the ventral

and dorsal lobes grew 9.1 and 3.7-fold, respectively, in one day. These findings suggest that localized perfusion into the ventral liver at E10.5 was a critical driver of subsequent liver growth (Fig. 1I and Supplementary Fig. 3).

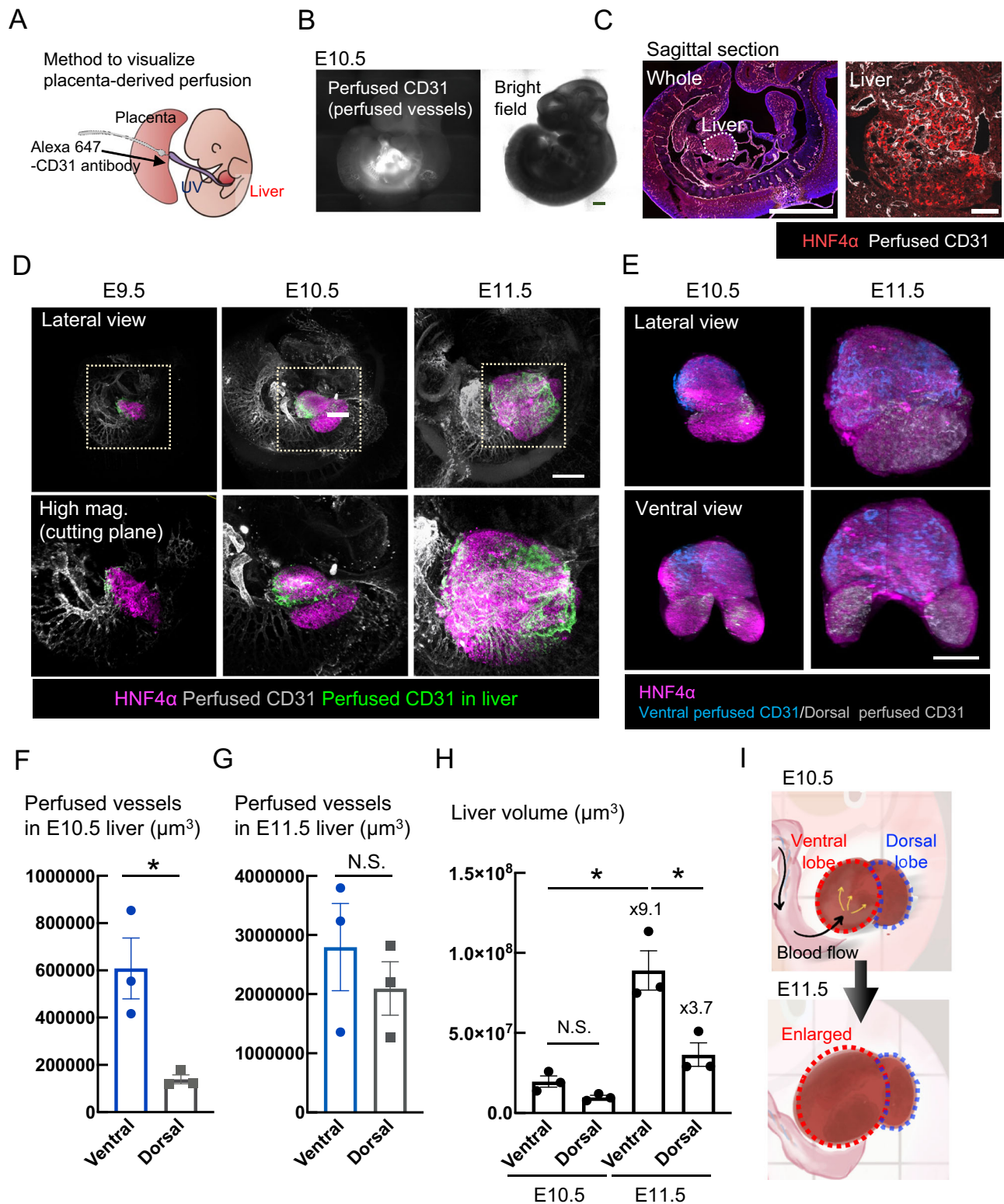
Then, the spatial relationship between the perfused blood vessels and proliferating hepatoblasts was examined next to investigate the contribution of hepatoblast proliferation to blood perfusion-dependent liver growth. Evaluation of liver sections collected 2 h after maternal EdU administration showed greater abundance of proliferating hepatoblasts in the ventral lobes compared to the dorsal lobes at E10.5 (Fig. 2A). Additionally, the proportions of proliferating hepatoblasts observed at E9.5 and E11.5 were comparable to those observed in the ventral lobes at E10.5 (Fig. 2A, B and Supplementary Fig. 4). Taken together, these findings supported our hypothesis that hepatoblast proliferation induced by placenta-derived blood contributed to the liver growth between E10.5 and E11.5.

Analysis of placenta-derived blood components

As the liver was perfused post-E10.5 and remarkably enlarged between E10.5 and E11.5, we examined which placenta-derived blood components (oxygen and placenta-derived factors) contribute to the enlargement of liver. First, pimonidazole²¹, a hypoxia marker that covalently binds to thiol-containing proteins at tissue PO₂ (Partial pressure of oxygen) levels below 10 mmHg, was detected with a specific antibody to examine whether the liver tissue was oxygenated by placenta-derived blood. Pimonidazole signal showed that the liver was under hypoxia at E9.5 when blood perfusion was yet to commence (Fig. 2C, D). The liver was, surprisingly, still under hypoxia at E10.5 despite blood perfusion, although it appeared to be oxygenated by E11.5 (i.e., pimonidazole-negative; Fig. 2C, D) suggesting that oxygen contributed to liver growth after this stage.

These findings were consistent with our metabolomics data to show that hepatoblasts altered their metabolic characteristics at E11.5 (Supplementary Fig. 5A). The expression of genes related to oxidative metabolism (e.g., TCA cycle, electron transport complex, and oxidative phosphorylation) was increased at E11.5 compared to E9.5 and E10.5 (Supplementary Fig. 5B). These findings suggest that hepatoblasts relied on oxygen to proliferate beyond E11.5. The expression of hepatocyte and hepatoblast markers were analyzed next to allow assessment of the association between hepatoblast differentiation and metabolic switching at E11.5. The findings showed that the hepatocyte markers were largely unaltered, while the hepatoblast markers were maintained between E9.5 to E11.5 (Supplementary Fig. 5C). Furthermore, single cell RNA sequencing (scRNAseq) data showed that all hepatic cells retained their hepatoblast properties (Supplementary Fig. 5D), suggesting that hepatoblasts continued to expand even after changes in the metabolic features of the liver at E11.5.

We hypothesize that hepatoblast expansion was enhanced in the blood-perfused ventral lobe (Figs. 1 and 2). Placenta-derived blood is considered to be crucial for fetal organ growth, as it delivers maternal blood components and various factors such as SOD3 produced in placenta¹⁶. Therefore, the growth factor response in the liver and the expression of growth factors in the placenta at E10.5 were examined using microarray data from a public database^{22,23} (Fig. 2E). Growth factors such as bone morphogenetic protein (BMP), fibroblast growth factor (FGF) and WNT that were derived from the mesenchymal tissues surrounding the liver [e.g., cardiac mesoderm (CM) and septum transversum mesenchyme (STM)] are known to contribute to liver growth between E8.25 and E9.5^{24–27}. In the current study, the BMP/FGF/WNT receptors were highly expressed at E9.5 and prominently decreased by E10.5 (Fig. 2E). Meanwhile, BMP/FGF/WNT ligands are not increased in sinus venosus (SV) and liver with STM between E9.5 and E10.5 (Supplementary Fig. 2G, H). However, the expression of growth factors in the placenta was increased at E10.5, and the genes associated with the responses to growth factors were also highly expressed in the



liver at this stage (Fig. 2E). Therefore, it can be assumed that placenta-derived factors were transiently associated with ventral liver growth between E10.5 and E11.5 through the promotion of hepatoblast expansion at E10.5 prior to oxygenation (Fig. 2F).

Effects of placenta-derived factors on hepatoblast expansion at E10.5

Kyoto Encyclopedia of Genes and Genomes (KEGG) pathway analysis was carried out using mouse E10.5 placenta and liver microarray data

to identify the signaling pathways contributing to hepatoblast expansion between E10.5 and E11.5 (Fig. 3A, B). Additionally, human GW5 placenta and human fetal liver microarray data were also analyzed^{22,23}. Among the enriched gene categories, the current study primarily focused on cytokine-cytokine receptor interactions and PI3K-Akt signaling pathways, which were commonly enriched in 4 groups and could be crucial for hepatoblast expansion (Fig. 3B). 23 placental ligands and 8 liver receptors were extracted (Fig. 3C), and the ligand-receptor pairings were searched using the CellTalkDB

Fig. 1 | Localized perfusion promotes the growth of the liver ventral lobe between E10.5 and E11.5. **A** Illustration of the method for visualizing placenta-derived perfused vessels using CD31 antibodies (Ab). **B** Confirmation of intravital CD31 Ab perfusion (gray). Scale bar = 1 mm. **C** Confirmation of CD31 Ab perfusion into the liver tissue sections. Images indicate perfused CD31 (gray) and HNF4 α (magenta). Scale bar = 500 μ m or 100 μ m. **D** Whole-mount imaging of perfused CD31 (gray) and HNF4 α (magenta) immunostaining at each stage. Perfused CD31 in the liver was visualized (green) using Imaris. Scale bar = 300 μ m. **E** Visualization of the perfused blood vessels in the ventral and dorsal lobes of the liver (blue or gray). Scale bar = 200 μ m. **F** Quantification of perfused blood vessels in the dorsal and ventral lobes of the liver at E10.5. Error bars are represented as SEM; Ventral ($n = 3$),

Dorsal ($n = 3$), two-tailed Student's t -test, Ventral vs. Dorsal (p -value = 0.0227). **G** Quantification of perfused blood vessels in the dorsal and ventral lobes of the liver at E11.5. Error bars are represented as SEM; Ventral ($n = 3$), Dorsal ($n = 3$), two-tailed Student's t -test, Ventral vs. Dorsal (p -value = 0.4640). **H** Quantification of the volume of the dorsal and ventral lobes of the liver at E10.5 and E11.5. Error bars are represented as SEM; Ventral ($n = 3$), Dorsal ($n = 3$), One-way ANOVA with Tukey's test, E10.5 ventral vs. E11.5 ventral (p -value = 0.001), E11.5 ventral versus E11.5 dorsal (p -value = 0.004). **I** Ventral liver growth between E10.5 and E11.5 followed by hepatoblast expansion induced by placenta-derived blood perfusion. Source data are provided as a Source Data file.

database. Five receptors (i.e., FGFR4, IL1RAP, IL13RA1, ACVR1, PDGFR β) were identified as the candidate associated with signaling pathways that could promote hepatoblast expansion (Fig. 3D). The effect of placental ligands on liver growth was evaluated by adding FGF2, IL1 α , IL13, InhibinB, and PDGFAB to E10.5 mouse liver embedded in gel under hypoxia to mimic in vivo oxygen conditions below 5%²⁸ (Fig. 3E). The oxygen concentration of the gel is reported to be -1 to 5%^{29,30}. Macroscopic images showed that addition of FGF2 and PDGFAB induced spreading of cells from the explant, which presumably consisted of mesenchymal cells (light gray region), while addition of IL1 α and InhibinB increased the area of liver parenchyma containing hepatoblasts (black region; Fig. 3E). Further quantification showed that IL1 α also significantly increased the area of the liver parenchyma (Fig. 3F). The region containing HNF4 α ⁺ hepatoblasts was measured using whole-mount immunostaining and the findings showed that the liver volume was significantly increased after the treatment of IL1 α when compared to the control group (Fig. 3E, F). IL1 α also increased the number of expanding hepatoblasts (Fig. 3E, F). Then, to demonstrate the placenta-specific IL1 α production, ELISA analysis was conducted using ex vivo tissue (placenta, heart, and liver as well as whole fetus) culture supernatant and showed placenta-specific IL1 α production, with no detectable production in the liver (containing STM), heart (sinus venosus) and fetus (Fig. 3G). Moreover, co-culture of placenta and liver confirmed the contribution of placental IL1 α to liver growth, as the placenta promoted liver growth during a 1-day culture (Supplementary Fig. 7A, B), which was suppressed by Nidanilimab (anti-IL1rap/IL-1R3; Supplementary Fig. 7A, B). These findings indicate that placenta-derived IL1 α promotes liver growth at E10.5.

The relationship between blood perfusion in the ventral lobes and the effects of IL1 α was assessed in vivo. Firstly, the localized expression of IL1 receptors (*Il1rap*) was evaluated using public spatial transcriptomic data³¹ (Fig. 3J). The findings showed higher *Il1rap* expression in the ventral lobe (perfused lobe) compared to the dorsal lobe, and this was further confirmed using IL1rap immunostaining (Fig. 3J, K). Next, to demonstrate the effect of placenta-derived IL1 α on ventral liver growth experimentally, IL1 receptor antagonist (IL1RA) was injected into pregnant mice to block IL1R signaling in fetus at E10.5. IL1RA suppressed the ventral liver growth from E10.5 to E11.5 (Fig. 3L, K). IL1RA also suppressed the hepatoblast expansion in the ventral liver (Fig. 3J, L). These findings suggest that flow of placenta-derived IL1 α into the ventral liver lobes at E10.5 promotes hepatoblast expansion (Fig. 3M).

To identify the IL1 α target cells in the liver, the cell population positive for *Il1rap* was analyzed using scRNAseq data between E9.5 and E11.5, revealing highly expression in mesenchymal cells (Supplementary Fig. 6A, B). Moreover, immunostaining of E9.5 to E11.5 liver showed that *Il1rap* expression was localized in hepatoblasts at E9.5 and in desmin⁺ mesenchymal cells at E10.5 and E11.5 (Supplementary Fig. 6C). Therefore, mesenchymal cells could potentially act as the IL1 α target at E10.5 when IL1 α promoted liver growth. Other receptors identified from the placenta-liver microarray data were uniformly expressed in the ventral and dorsal lobes of the liver at E10.5 (Supplementary Fig. 6A, B).

IL1 α promoted human iPSC-derived liver organoid growth

Examination of mouse embryos and explants revealed that placenta-derived factor promoted fetal liver growth under hypoxia. Based on these findings, a protocol was established to increase the size of hiPSC-liver organoids wherein the placenta-derived factor, IL1 α , was added to a hiPSC liver organoid culture consisting of hiPSC-hepatoblasts (HE), endothelial cells (EC), and mesenchymal cells (MC)^{4,22}. hiPSC-HE began to express low levels of ALB on day 3 of organoid culture, similar to mouse E10.5 hepatoblasts (ALB^{low} Hep.; Supplementary Fig. 8A). To recapitulate mouse liver growth at E10.5, the effects of placenta-derived factors on hiPSC liver organoids containing ALB^{low} HNF4 α ⁺ hepatoblasts were examined under hypoxia (Fig. 4A). Ligands identified during analysis of mouse, human placenta, and liver microarray data (Fig. 3) were added to the hiPSC-liver organoid gel culture for one week, and the findings showed that the area of Kusabira-Orange labeled iPSC-HE (KO-HE) increased in the IL1 α -treated group compared to the control group, suggesting that IL1 α promoted hepatoblast expansion (Fig. 4B and Supplementary Fig. 8B). Furthermore, whole-mount immunostaining showed that the expanding hepatoblasts (Ki67⁺KO⁺) and liver organoid volume (HNF4 α ⁺ hepatoblast region) increased in the IL1 α -treated group (Fig. 4B). These findings indicate that IL1 α promotes hiPSC-liver organoid and mouse fetal liver growth along with hepatoblast expansion.

To demonstrate that hepatoblasts retained their characteristics in IL1 α -treated organoids, colony assays were conducted. Single or small clusters of cells from IL1 α pre-treated organoids were embedded in Matrigel and cultured for 3 days (Fig. 4C). The findings showed that IL1 α pre-treated KO-HE colonies were significantly expanded compared to the control group (Fig. 4D, E) and also exhibited hepatoblast markers (ALB⁺CK19⁺)³² after expansion (Fig. 4E). Additionally, we also confirmed that HEs showed hepatoblast markers in IL1 α -treated hiPSC-liver organoids (Supplementary Fig. 8C). These results suggest that hiPSC-hepatoblasts in liver organoids treated with IL1 α retained their characteristics.

In silico analysis of IL1 receptor-mediated signaling

In order to gain insight into the mechanisms by which IL1 α promotes hepatoblast expansion in hiPSC-liver organoids, the target cell types were analyzed using previously published scRNAseq data for hiPSC-HEs, ECs, and MCs before and after organoid formation³. The findings showed that IL1RAP, IL1R1, and IL1R2 were barely expressed in hiPSC-HEs, ECs and MCs, while IL1RAP and IL1R1 were mainly expressed in MCs of organoids (Org-MCs) (Fig. 4F). These findings suggested that similar to mouse in vivo data (Supplementary Fig. 6B), the IL1 α receptors are mainly expressed in mesenchymal cells during organogenesis and IL1 α acts on MCs to promote hepatoblast expansion in hiPSC-liver organoids.

To further investigate the relationship between IL1 receptor-mediated signaling and hepatoblast expansion, we performed ingenuity pathway analysis (IPA) on the organoid-constituting cells. After incubating hiPSC-liver organoids with or without IL1 α for one week, those containing fluorescent protein expressed cells (KO-HE, double negative-EC, GFP-MC) were dispersed and three types of cells were collected by FACS (Fig. 4F). IPA using RNAseq data for HEs, ECs, and

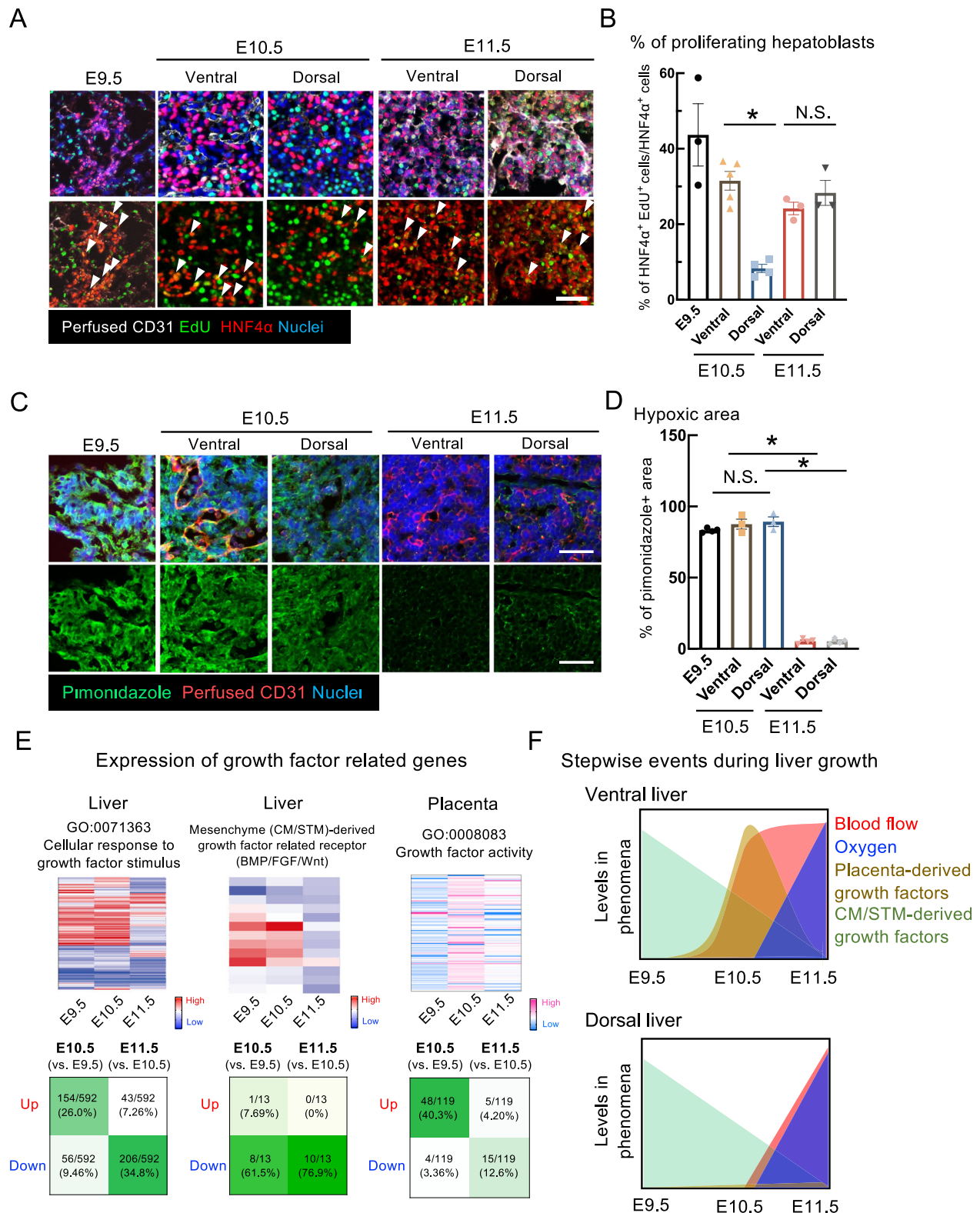
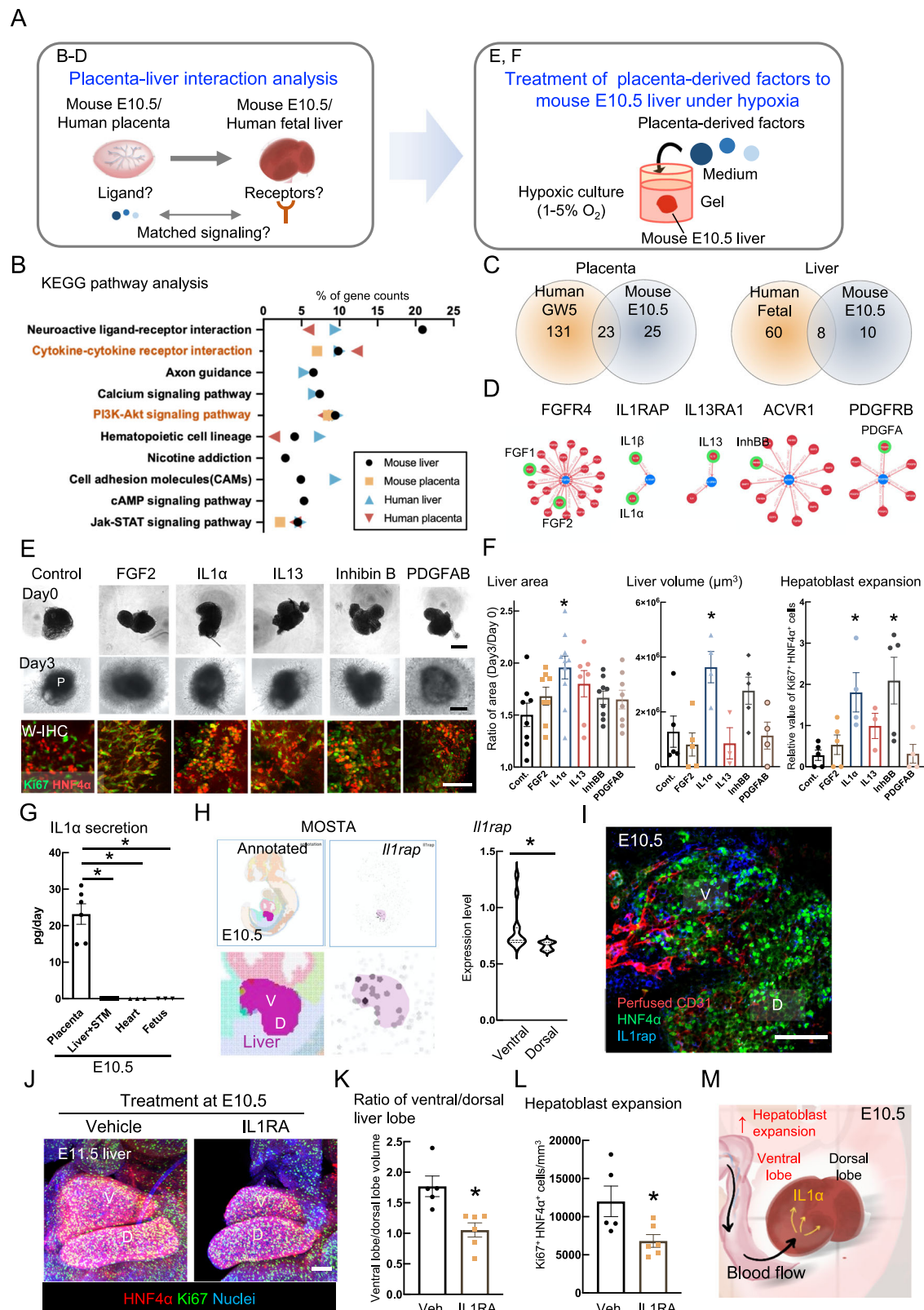


Fig. 2 | Hepatoblast expansion induced by placenta-derived blood perfusion under hypoxia. A Images of perfused CD31 and HNF4α/EdU immunostaining in each stage. Scale bar = 50 μm. **B** Quantification of hepatoblast expansion by counting the number of HNF4α⁺EdU⁺ cells at each stage. Error bars are represented as SEM; E9.5 (*n* = 3), E10.5 Ventral (*n* = 5), E10.5 Dorsal (*n* = 4), E11.5 Ventral (*n* = 3), E11.5 Dorsal (*n* = 3), One-way ANOVA with Tukey's test, E10.5 Ventral vs. E10.5 Dorsal (*p*-value = 0.002), E11.5 Ventral vs. E11.5 Dorsal (*p*-value = 0.9467). **C** Oxygen level in the liver at each stage. Pimonidazole indicated hypoxic regions (green). Scale

bar = 50 μm. **D** Quantification of pimonidazole positive regions in the liver. Error bars are represented as SEM; E9.5 (*n* = 4), E10.5 Ventral (*n* = 3), E10.5 Dorsal (*n* = 3), E11.5 Ventral (*n* = 4), E11.5 Dorsal (*n* = 4), One-way ANOVA with Tukey's test, E10.5 ventral versus E11.5 ventral (*p*-value < 0.0001), E10.5 dorsal versus E11.5 dorsal (*p*-value < 0.0001). **E** Microarray data of growth factor-related gene expression in placenta or liver. **F** Putative spatiotemporal interactions between liver and placenta. Placenta-derived blood containing factors perfuses into the ventral lobe of the liver. Source data are provided as a Source Data file.



MCs (Fig. 4F, G) showed that IL1R-mediated signaling eventually activated inflammatory and IGF1 upregulating pathways. Specifically, it was predicted that the inflammatory signaling pathway was accompanied by the expression of cytokines such as LCN2, CCL20, and C3 (Model #1, blue dotted line), while another signaling pathway led to expression of IGF1 through CSF3 (Model #2, gold dotted line; Fig. 4G and S9). To test the predictions, the effect of inhibitors on these pathways (LCN2, IGF-1, C3 and CCL20) was evaluated. Among them, CCR6 antagonist, which

blocks CCL20 signaling, suppressed hiPSC-hepatoblast expansion induced by IL1 α (Fig. 4H). Previous research has shown that serum amyloid A1 (SAA1) induces CCL20 secretion^{33,34}. Therefore, it was estimated SAA1 is upstream of CCL20. In IL1 α -treated hiPSC-liver organoids, EC and MC strongly expressed SAA1 (Fig. 4I). Additionally, SAA1 induced CCL20 secretion from hiPSC-liver organoids (Fig. 4J). These findings suggest that IL1 α contributes to hiPSC-hepatoblast expansion through SAA1-TLR2-CCL20-CCR6 signaling pathways.

Fig. 3 | Placenta-derived IL1 α promotes hepatoblast expansion at E10.5.

A Schematic overview of placenta-liver interaction analysis. **B** KEGG pathway analysis using human and mouse placenta and liver microarray data. **C** Extraction of enriched genes in humans and mice, as shown in the Venn diagram. **D** Ligands and receptors with matched signaling using CellTalkDB. **E** Effect of placental ligands on fetal liver culture. Whole-mount staining three days after culture. P: Parenchyma. Scale bar = 500 μ m or 100 μ m. **F** Liver area calculated using macro-images during culture. Error bars are represented as SEM; Control ($n = 8$), FGF2 ($n = 8$), IL1 α ($n = 10$), IL13 ($n = 7$), InhBB ($n = 9$), PDGFAB ($n = 8$), One-way ANOVA with Tukey's test, IL1 α versus Control (p -value = 0.0196). Liver volume calculated using whole-mount images. Error bars are represented as SEM; Control ($n = 5$), FGF2 ($n = 5$), IL1 α ($n = 4$), IL13 ($n = 3$), InhBB ($n = 5$), PDGFAB ($n = 4$), two-tailed Mann-Whitney U-test, IL1 α versus Control (p -value = 0.0159). Hepatoblast expansion calculated using whole-mount images. Error bars are represented as SEM; Control ($n = 5$), FGF2 ($n = 5$), IL1 α ($n = 4$), IL13 ($n = 3$), InhBB ($n = 5$), PDGFAB ($n = 4$), two-tailed Mann-Whitney U-test, IL1 α versus Control (p -value = 0.0159), InhBB versus Control

(p -value = 0.0159). **G** IL1 α production from isolated each tissue. Error bars are represented as SEM; Placenta ($n = 6$), Liver+STM ($n = 4$), Heart ($n = 3$), Fetus ($n = 3$), One-way ANOVA with Tukey's test, Placenta versus each group (p -value < 0.0001). **H** Examination of IL1rap expression in the ventral and dorsal lobes of the liver using MOSTA. Error bars are represented as SEM; Ventral ($n = 11$), Dorsal ($n = 6$), two-tailed Mann-Whitney U-test, Ventral versus Dorsal (p -value = 0.0063). Scale bar = 500 μ m or 100 μ m. **I** Examination of IL1rap expression in the ventral and dorsal lobes of the liver using immunostaining. Scale bar = 100 μ m. **J** E11.5 whole liver after IL1 receptor antagonist (IL1RA) treatment at E10.5. Scale bar = 100 μ m. **K** Ratio of ventral/dorsal liver lobe after IL1RA treatment. Error bars are represented as SEM; Vehicle ($n = 5$), IL1RA ($n = 6$), two-tailed Mann-Whitney U-test, IL1RA versus Vehicle (p -value = 0.0043). **L** Hepatoblast expansion after IL1RA treatment. Error bars are represented as SEM; Vehicle ($n = 5$), IL1RA ($n = 6$), two-tailed Student's t -test, IL1RA versus Vehicle (p -value = 0.0314). **M** Hepatoblast expansion occurs in the ventral liver lobe after perfusion with placenta-derived IL1 α at E10.5. Source data are provided as a Source Data file.

Sequential IL1 α and oxygen treatment promotes hiPSC-liver organoid growth

Hepatoblasts proliferate in the oxygenated mouse liver after IL1 α -induced hepatoblast expansion between E10.5 and E11.5 (Figs. 1 and 2). To examine whether oxygen specifically promoted proliferation of hiPSC-hepatoblasts, hiPSC-liver organoids containing ALB^{low}HNF4 α ⁺ and ALB^{high}HNF4 α ⁺ hepatoblasts were incubated under different concentrations of oxygen. The findings showed promotion of the proliferative capacity of ALB^{high}HNF4 α ⁺ hepatoblasts but not ALB^{low}HNF4 α ⁺ hepatoblasts in high ambient O₂ (40% oxygen), which is predicted 7.6% oxygen in gel³⁰ (Supplementary Figs. 10A–C). However, the proliferative capacity of ALB^{high}HNF4 α ⁺ hepatoblasts did not increase in higher ambient O₂ (80% oxygen), which is predicted 15.3% oxygen in gel³⁰ (Supplementary Fig. 10D), suggesting that oxygen specifically regulated the proliferation of ALB^{high} hepatoblasts and a concentration of 40% was sufficient to induce this effect.

Hepatoblasts were seen to exhibit ALB^{high} status upon exposure to oxygen (Fig. 2 and Supplementary Fig. 8A), suggesting that hepatoblasts exposed to IL1 α underwent simultaneous proliferation and differentiation. The expression of ALB was evaluated in hiPSC-hepatoblasts that proliferated in the presence of IL1 α . IL1 α -treated and control hiPSC-liver organoids exhibited higher ALB expression on day 7 compared to day 0, and no differences were observed between the groups (Supplementary Fig. 10E). These findings suggest that the shift from ALB^{low} to ALB^{high} is a spontaneous event, and IL1 α plays a major role through promotion of hepatoblast expansion during liver organoid culture (Supplementary Fig. 10F). Thereafter, IL1 α and oxygen were sequentially introduced to hiPSC-liver organoids (Fig. 5A), and this continuous treatment increased Ki67⁺HNF4 α ⁺ proliferating hepatoblasts (Fig. 5A, B). Liver organoid size was slightly increased after addition of IL1 α or oxygen alone, while combined treatment with both increased the liver organoid volume by ~5-fold when compared to the control group (Fig. 5C). Furthermore, IL1 α /oxygen-treatment also induced functional expression (hALB secretion) of hiPSC-liver organoids (Fig. 5D). Moreover, hiPSC-hepatoblasts exhibited the high expressions of both hepatocyte and hepatoblast markers in IL1 α /oxygen-treated hiPSC-liver organoid (Fig. 5E). These findings demonstrated that sequential treatment with placenta-derived factors promoted hiPSC liver organoid growth and function. Overall, the current study achieved prominent growth of hiPSC liver organoids driven by hepatoblast expansion through recapitulation of molecular events governed by extrinsic factors in mouse fetal liver.

Discussion

The current study focused on placenta-fetal organ interactions to identify placenta-derived factors that promote progenitor expansion, a crucial process during organ growth. Our data demonstrated that recapitulation of the transient environment by supplying placenta-

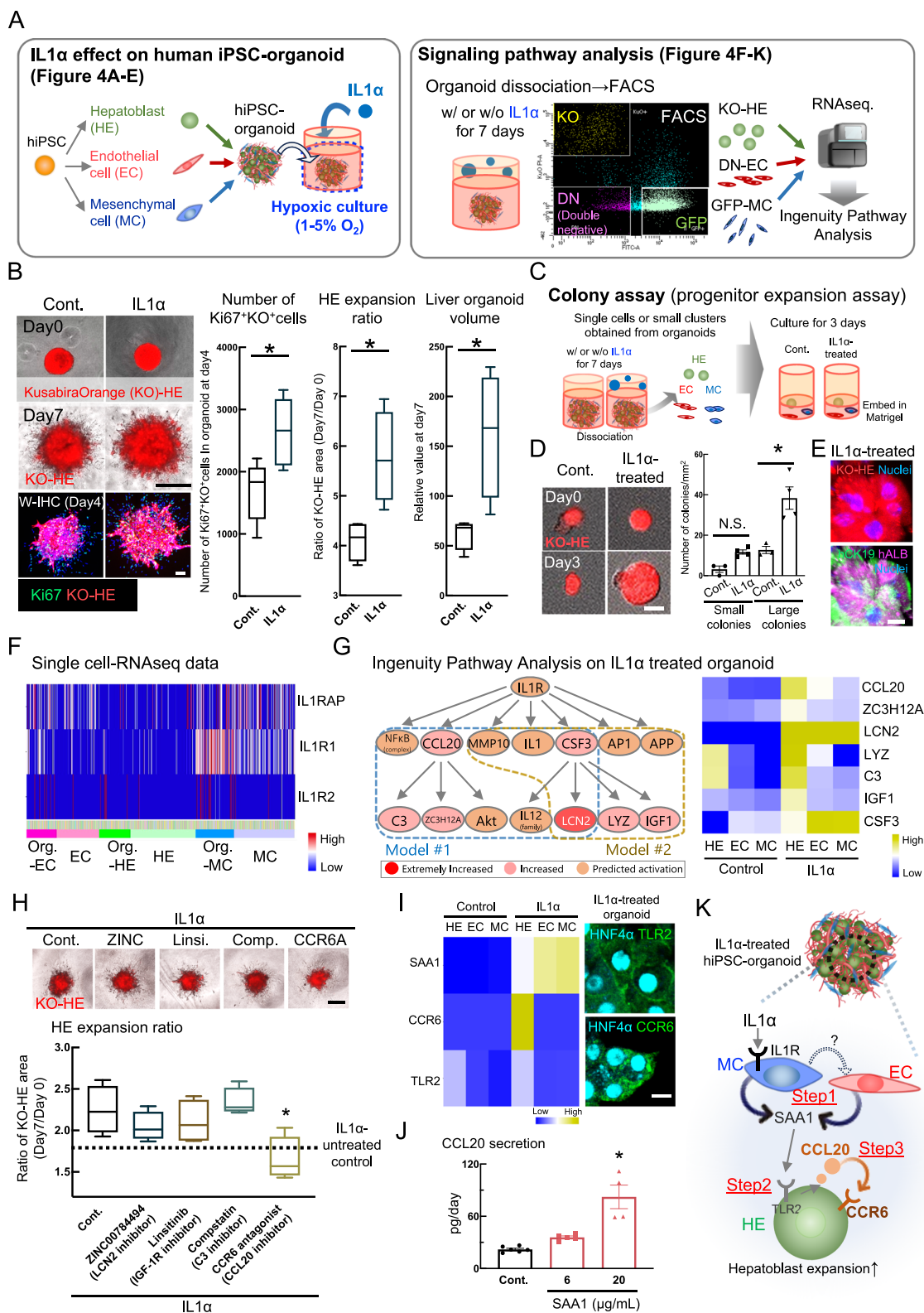
derived factor under hypoxia was essential for progenitor expansion in hiPSC-organoid culture. Considering that progenitor expansion is a common process in various organs as well as liver, the other hiPSC-organoid growth may also be promoted by progenitor expansion induced by any placenta-derived factors under hypoxia.

A recent study suggested that organ size was determined by exogenous signals from the in vivo environment as well as cell-autonomous endogenous signals³⁵. Blood perfusion is a primary exogenous signal involved in organ growth by delivering nutrients and oxygen from the placenta to the organs¹⁵. However, there is limited evidence on when the placenta-derived blood starts to perfuse fetal organs and which blood components regulate the progenitor expansion and organ size. Therefore, we developed a method to visualize placenta-derived blood perfusion, wherein the labeled perfused vessels and organ growth were evaluated using 3D imaging techniques. Rapid enlargement of the perfused ventral lobes (but not the hypoperfused dorsal lobes) of the liver occurred by E11.5 prior to oxygenation (Fig. 1E–H). Given that the results in current study using sagittal histological sections collected from late-stage fetuses (Figure S3) and the ventral lobes typically develop into the middle lobes (i.e., the largest lobes) in adulthood³⁶, it is possible that blood perfusion during early organogenesis can determine the size of the liver lobes in adults.

We found the transient stage that the liver is not oxygenated, although the tissue is perfused by placenta-derived blood at E10.5 (Fig. 2C, D). This could be attributed to hypoxic condition in placenta at E10.5 considering a deficiency of HIF1 β (ARNT), which dimerizes with HIF1 α induces placental hypoplasia³⁷. Hypoxia has been shown to play an important role in fetal organ growth as well as placenta, although cultures under hypoxic conditions alone failed to induce progenitor expansion²⁸. Therefore, we assume that placenta-derived blood may supply soluble factors promoting progenitor expansion under hypoxia.

Mice lacking functional IL1r1 or IL1rap, which are subunits of IL1R, have been reported to exhibit normal development^{38,39}. However, it remains unknown whether IL1R signaling-deficient mice show any phenotypes during organogenesis. In this study, we demonstrated that IL1 α is specifically produced by placenta at E10.5, and pharmacological inhibition of IL1 α signaling results in a significant reduction in the size of the ventral liver lobe. This suggests that normal liver growth between E10.5 and E11.5 depends on IL1 α signaling (Fig. 3). Therefore, it would be intriguing to investigate how the defective progenitor expansion affects the liver development or homeostasis in mice lacking functional IL1R signaling, such as a placenta-specific IL1 α knockout or liver-specific IL1R knockout mice in future studies.

Using hiPSC-liver organoid system, we demonstrated the downstream of IL1R involved in hepatoblast expansion (Fig. 4). Previous studies have shown that IL1 treatment induces SAA1 expression in human hepatocyte cell lines and SAA1 treatment enhances CCL20 production in monocytes^{33,34}. We suggested IL1 α -induced SAA1-



TLR2-CCL20-CCR6 pathway is involved in human hepatoblast expansion. More specifically, SAA1 derived from EC and MC induces CCL20 expression in HEs, leading to HE expansion in an autocrine manner (Fig. 4K). Previous research has indicated that CCR6 is involved in cell proliferation⁴⁰. These findings suggest that IL1 α likely promotes hepatoblast expansion in hiPSC-liver organoids at least in part through SAA1-TLR2-CCL20-CCR6 related inflammatory signaling pathways.

In conclusion, our study recapitulated *in vivo* progenitor expansion in hiPSC-liver organoids by the mimicry of placenta-liver interaction through fetal blood under hypoxia. Although it is widely known that the vascular endothelial cell contributes to organogenesis^{41,42}, it remains largely unexplored about the impact of blood flow, including mechanical stress and flow-induced angiocrine factors, and its components (such as endocrine factors derived from distal organs, oxygen, and so on) to the organ growth. Our analysis unveiled the sequential

Fig. 4 | IL1 α promotes hiPSC-derived liver organoid growth. **A** Schematic overview of hiPSC-liver organoid culture and subsequent analysis. **B** Effect of IL1 α on hiPSC-liver organoid culture. KO (Kusabira–Orange) indicates hiPSC-hepatoblasts (KO-HE). Whole-mount staining three days after organoid culture. Scale bar = 500 μ m or 100 μ m. Quantification of liver volume using the HNF4 α ⁺ regions. Box plots show the minimum value to maximum value. Error bars are represented as SEM; Control ($n = 4$), IL1 α ($n = 4$), two-tailed Mann–Whitney U-test, IL1 α versus Control (p -value = 0.0286). **C** Colony assay using single or small cluster of cells derived from organoids with or without IL1 α . **D** Ratio of HE colony areas with and without IL1 α pre-treatment. Error bars are represented as SEM; Control small colonies ($n = 3$), IL1 α small colonies ($n = 4$), Control large colonies ($n = 3$), IL1 α large colonies ($n = 4$), One-way ANOVA with Tukey's test, IL1 α small colonies versus Control small colonies (p -value = 0.3600), IL1 α large colonies versus Control large colonies (p -value = 0.0019). **E** The expression of ALB⁺CK19⁺ in IL1 α pre-treated HE colony. Scale bar = 10 μ m. **F** Expression of IL1 receptor related genes using single cell RNA-seq

data set (Camp JG et al. *Nature* 2017). **G** Ingenuity Pathway Analysis (IPA) in organoid using RNAseq data. **H** Effects of inhibitors against each pathway estimated by IPA on HE expansion for 7 days. Box plots show the minimum value to maximum value. Error bars are represented as SEM; Control ($n = 4$), ZINC00784494 ($n = 4$), Linsitinib ($n = 4$), Compstatin ($n = 4$), CCR6 antagonist ($n = 4$), One-way ANOVA with Tukey's test, CCR6 antagonist versus Control (p -value = 0.0219). Scale bar = 500 μ m. **I** Gene expression of *SAAI*, *CCR6* and *TLR2* on HE, EC and MC. Immunostaining of CCR6 and TLR2. Scale bar = 10 μ m. **J** CCL20 secretion from hiPSC-liver organoid after SAA1 treatment. Error bars are represented as SEM; Control ($n = 4$), SAA1 6 μ g/mL ($n = 4$), SAA1 20 μ g/mL ($n = 4$), One-way ANOVA with Tukey's test, SAA1 20 μ g/mL versus Control (p -value < 0.0001). **K** Estimated cell-cell interaction within hiPSC-liver organoid after IL1 α treatment. Hepatoblast expands through IL1 α -induced SAA1-TLR2-CCL20-CCR6 signaling. Source data are provided as a Source Data file.

supply of IL1 α under hypoxia and oxygen as blood flow components contribute to liver growth in mouse as well as human organoids. However, complete recapitulation of the in vivo environment was not achieved as the hiPSC-liver organoid was cultured under static conditions. Future studies should aim to construct a human organoid perfusion culture system and efficiently provide fetal blood components, including placenta-derived factors and oxygen, to facilitate in vitro generation of human organs.

Methods

Mice

Pregnant C57BL/6J mice were purchased from Japan SLC. All animal experiments were approved by the Institutional Animal Care and Use Committee at the University of Tokyo (PA22-05). All mice were housed under the University of Tokyo animal center standard with a 12-h dark/light cycle, an ambient temperature of $22 \pm 2^\circ\text{C}$, and a relative humidity of $50 \pm 10\%$.

Visualization of perfused vessels in the fetus

For the microinjection, 34-gauge needle (Terumo) was connected to the joint tube (PE tube; inner diameter: 0.28 mm, outer diameter: 0.61 mm, BD) attaching to a thicker tube (PE tube; inner diameter: 0.40 mm, outer diameter: 0.80 mm). Before the injection, the needle and tube were filled with Alexa647-conjugated CD31 antibody (Biolegend) in PBS (1:5 dilution) using a micro-syringe (SGE). The pregnant mice were anesthetized using 0.3 mg/kg of medetomidine, 4.0 mg/kg of midazolam, and 5.0 mg/kg of butorphanol. Under a surgical microscope, the fetus was exposed, and needle was inserted into the umbilical vein between the placenta and fetus, and 20–30 μ L of the solution was slowly injected into the vessel over a duration of 1 min. Fetus that exhibited fluorescent signals was collected for analysis. The antibody injection procedure is shown in Supplementary Movie 1.

Evaluation of hypoxic area

Pimonidazole (HypoxyprobeTM-1, HPX) was injected intraperitoneally into the pregnant mice, and the fetuses were collected after 2 h²¹. Immunostaining of pimonidazole in the tissue sections was carried out as per the manufacturer's protocol, and the hypoxic area was evaluated using Fiji (NIH).

Labeling of proliferative cells

EdU (thymidine base analog, Thermo Fisher Scientific) was diluted in PBS to a concentration of 1 mM before being injected intraperitoneally into pregnant mice. After 2 h, the pregnant mice were anesthetized, and the fetal mice were injected with CD31 Ab. After fixation and cryosectioning of the embryos, the EdU Click-iTTM assay was performed as per the manufacturer's protocol (Thermo Fisher Scientific). After the confirmation of the fluorescence signal of perfused anti-CD31 antibody in the fetus, histological analysis was performed using the whole liver

section of E9.5 and E11.5 (1 section/sample) and E10.5 (2 or 3 sections/sample). The ratio of HNF4 α and EdU double positive cells per total HNF4 α positive cells was calculated by counting cells positive for HNF4 α and EdU in the whole area of each liver section ($>20,000 \mu\text{m}^2$).

Microarray and pathway analysis

The liver microarray data was re-analyzed (accession code is [GSE106465](#)) using the Whole Mouse Genome Agilent 4344 K v2 Oligonucleotide Microarray or the Whole Human Genome Agilent 4344 K v2 Oligonucleotide Microarray (Agilent Technologies) platforms², while the placenta microarray data was re-analyzed (accession code is [GSE100053](#)) using the Illumina MouseRef-8 v2.0 expression BeadChip or the Illumina HumanHT-12 V4.0 expression BeadChip platforms²³. Data analysis was performed using the Subio Platform, version 1.24.5853 (Subio).

KEGG pathway analysis was carried out using a list of differentially expressed genes (DEGs) identified from the microarray data using the Database for Annotation Visualization and Integrated Discovery (DAVID). Upregulated genes (i.e., 2-fold increase in mouse liver at E10.5 compared to E9.5 or human fetal liver versus adult liver or 1.2-fold increase in mouse placenta E10.5 versus E9.5 or human placenta GW5 versus GW4 with raw signals) were analyzed as DEGs.

Blood flow suppression

The pregnant mice were anesthetized using 0.3 mg/kg of medetomidine, 4.0 mg/kg of midazolam, and 5.0 mg/kg of butorphanol. Maternal blood flow into the fetal mice was suppressed through bilateral uterine artery ligation using 4–0 sutures (Natsume), as reported previously⁴³. After the closure of abdominal wall, 0.75 mg/kg of Antisedan was treated to awaken the mice from anesthesia. After 6 h, the fetal mice were collected while the pregnant mice were anesthetized. In Sham group, the abdominal wall was incised under anesthesia, and the uterus was exposed using the same procedures as in the ligation group. We confirmed that there is no significant difference in embryo size between sham and ligation group.

Mouse fetal liver culture

Embryos were collected in Opti-MEM (Opti-MEMTM Reduced Serum Medium, GlutaMAXTM Supplement) containing 1% penicillin-streptomycin. After the Collagen (Cultrex Rat Collagen I, R&D)/Matrigel (Corning) solidification in plates, the dissected fetal livers were then transferred on solid gels and then overlaid with unsolid gels for sandwich culture. After incubation for 30 min at 37°C , Opti-MEM containing 2.5% FBS, 1% penicillin-streptomycin, and placenta-derived factors were added. After three days of culture, the liver tissues were fixed in 4% PFA at 4°C and used for whole-mount immunostaining. Recombinant mouse FGF-basic/FGF2 (R&D), recombinant mouse IL1 α /IL-1F1 (R&D), recombinant mouse IL-13 (R&D), recombinant mouse Inhibin Beta B (CLOUD-CLONE CORP), and recombinant mouse

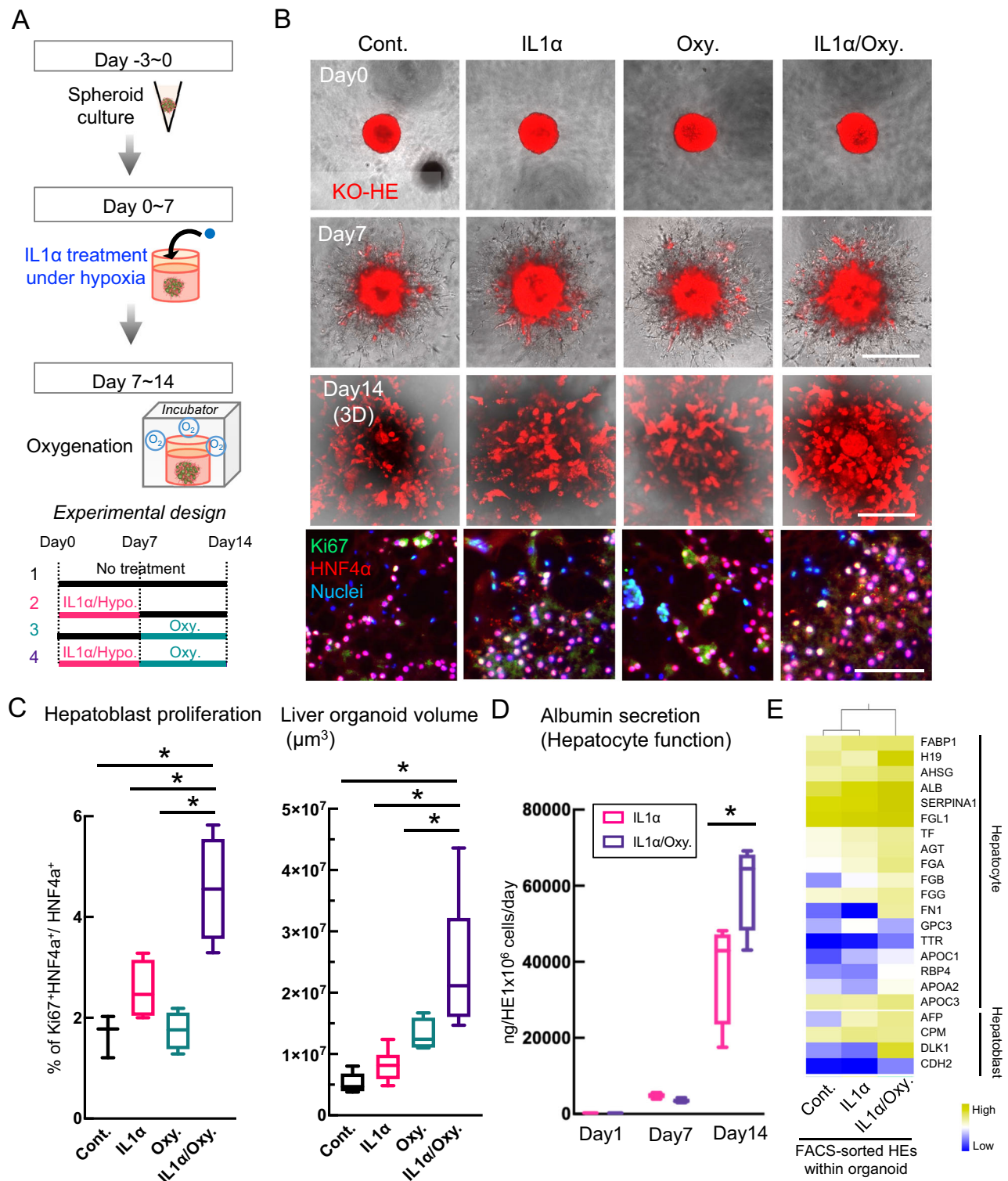


Fig. 5 | Oxygen enhances IL1α-induced hiPSC-liver organoid growth. **A** Culture protocol of hiPSC-liver organoid based on the analysis of liver development. **B** Effect of IL1α and oxygen (Oxy) on hiPSC-liver organoid. KO-HE was observed in 3D on day 14. Ki67 (green) and HNF4α (red) immunostaining using hiPSC-liver organoid tissue sections. Scale bar = 500 μm or 100 μm. **C** Quantification of hepatoblast proliferation indicated by HNF4α⁺Ki67⁺ on day 14. Box plots show the minimum value to maximum value. Error bars are represented as SEM; Control ($n = 3$), IL1α ($n = 4$), Oxy ($n = 4$), IL1α/Oxy ($n = 4$), One-way ANOVA with Tukey's test, IL1α/Oxy versus Control (p -value = 0.0008), IL1α/Oxy versus IL1α (p -value = 0.0072), IL1α/Oxy versus Oxy (p -value = 0.0005). Quantification of hiPSC-liver organoid volume on day 14. Error bars

are represented as SEM; Control ($n = 6$), IL1α ($n = 6$), Oxy ($n = 4$), IL1α/Oxy ($n = 6$), One-way ANOVA with Tukey's test, IL1α/Oxy versus Control (p -value = 0.0002), IL1α/Oxy versus IL1α (p -value = 0.0010), IL1α/Oxy versus Oxy (p -value = 0.0437). **D** Quantification of hALB secretion from hiPSC-liver organoids over time. Box plots are shown the minimum value to maximum value. Error bars are represented as SEM; IL1α day1 ($n = 4$), IL1α/Oxy day1 ($n = 4$), IL1α day7 ($n = 4$), IL1α/Oxy day7 ($n = 4$), IL1α day14 ($n = 4$), IL1α/Oxy day14 ($n = 4$), two-tailed Student's t -test, IL1α/Oxy day14 versus IL1α day14 (p -value = 0.0485). **E** Gene expressions of hepatocyte and hepatoblast markers on HE sorted from IL1α/Oxy-treated hiPSC-liver organoid. Source data are provided as a Source Data file.

PDGF-AB (R&D) were used as placenta-derived factors. The dissected fetal liver tissues were co-cultured with placenta in above conditions. Nidanilimab (Anti-IL-1RAP/IL-1R3) (Selleck, A2444) was used to block the IL1 α signal.

MOSTA (mouse organogenesis spatiotemporal transcriptomic atlas) analysis

Data from the ventral and dorsal lobes of the liver (STDS0000058_E10.5_E1S3.MOSTA data) were selected for comparison of the expression of receptors. Additionally, gene expression was analyzed in the liver-annotated area on the website (<https://db.cngb.org/stomics/mosta>)³¹.

IL1 receptor antagonist (IL1RA) treatment

IL1RA (MERCK) 10 mg/kg⁴⁴ was injected intraperitoneally into pregnant mice at E10.5. After 1 day, fetuses were collected for analysis. The volume of ventral and dorsal lobes was calculated using reconstructed 3D images using Imaris. Number of HNF4 α ⁺ Ki67⁺ cells was also calculated using reconstructed 3D images.

hiPSC culture and HE/EC/STM differentiation

The hiPSC lines (Ff01), provided by the Center for iPS Cell Research and Application, Kyoto University (CiRA), were maintained on Laminin 511 E8 fragment (iMatrix-511, Nippi)-coated dishes in StemFit AK02N (Ajinomoto)^{3,22}. For in vitro liver imaging analysis, the cells were infected with retroviruses expressing genes encoding Kusabira-Orange (KO), as described previously⁴⁵. The use of hiPSCs was approved by the ethics committee of the University of Tokyo (2023-102-0305, 2023-101-0308). Previously established protocols were used for HE/EC/STM differentiation^{22,46}.

hiPSC-liver organoid culture

hiPSC-liver organoids were formed from hiPSC-HE/EC/STMs using a previously established protocol with minor modifications²². The hiPSC-liver organoids were formed using PrimeSurface[®] plates (Sumitomo) to ensure uniformity in size with mouse fetal liver. After three days of plate culture, the hiPSC-liver organoids were embedded in Collagen/Matrigel, and DMEM(2.5% FBS, 100 nM Dexamethasone, 20 ng/mL Oncostatin M)/VEG1 (plus supplement without FBS) medium was added to the gel. Thereafter, the gel-embedded culture was treated with placenta-derived factors such as recombinant human FGF basic (Wako), recombinant human IL1 α (PeproTech), recombinant human IL-13 (R&D), recombinant human Inhibin beta B (Abcam), recombinant human PDGF-AA (R&D), or oxygen for 14 days.

The oxygen content in gels is 1–5% during unoxxygenated culture^{29,30}. For high ambient O₂ culture, the incubator was filled with O₂ 40% or 80%, and the oxygen content in gels was estimated be around 7.6% and 15.3%³⁰.

Inhibitors were used as follows. ZINC00784494 (MedChemExpress, HY-148364), final concentrations: 10 μ M, Linsitinib (OSI-906) (Selleck, S1091), final concentrations: 0.1 μ M, Compstatin (Selleck, S8522), final concentrations: 50 μ M, CCR6 antagonist 1 (MedChemExpress, HY-151435), final concentrations: 50 μ M. Human Apo-SAA (PeproTech, 300-13) recombinant was also used.

Colony assay

Single or small clusters of cells were obtained from organoids dissociated using collagenase, pronase, and DNase⁴⁷. The cells were then embedded in Matrigel and cultured for three days, after which the number of KO-HE colonies were counted by size (i.e., small: <100 μ m² and large: \geq 100 μ m²)⁴⁸.

Whole-mount immunostaining and clearing

The fetal mice were fixed in 4% PFA at 4 °C overnight, after which they were washed using 0.1% Tween in PBS. The detergent CHAPS (3-[(3-

cholami- dopropyl) dimethylammonio]-1-propanesulfonate)/ NMDEA (N-methyldiethanolamine) was used to increase antibody permeability into the tissues⁴⁹. The samples were incubated for 1–2 h at 37 °C, washed with 0.1% Tween in PBS, blocked with Protein Block (Agilent), and incubated with primary antibodies diluted in Protein block in PBS (1:10 dilution) for 4 days at 4 °C. Thereafter, they were washed and fluorescent dye-conjugated secondary antibodies were applied to the samples overnight at 4 °C. The primary antibodies used have been listed in Supplementary Table 1.

For clearing, the samples were dehydrated in 50% (vol/vol) methanol/PBS and moved in 100% methanol. The methanol was then replaced with 50% (vol/vol) benzyl alcohol/benzyl benzoate (BABB)/methanol and, finally, with 100% BABB⁵⁰.

3D image analysis

The samples were placed in glass-bottom dishes (Matsunami) and observed using a confocal microscope SP8 (Leica Microsystems). Whole mice or hiPSC-liver organoid scanning was carried out using the water immersion objectives in tiling mode. The Imaris software (Bit-plane) was used for reconstruction of 3D images, which were then visualized in masked regions that were selected in 2D sequential images using manual surface rendering. The ROIs included HNF4 α ⁺ and KO⁺ areas, and volume was calculated using the auto surface rendering regions.

Tissue processing and immunostaining

The tissues were fixed in 4% PFA for 24 h at 4 °C, cryoprotected in 30% sucrose for 24 h at 4 °C, and then embedded in optimal cutting temperature compound. Sagittal sections were placed on MAS-coated slides (Matsunami) for immunostaining, and Protein Block, Serum-Free (DAKO) was used for blocking to suppress non-specific reactions. The tissue sections were then incubated with primary antibodies overnight at 4 °C and then with secondary antibody Alexa Fluor (Thermo Fisher Scientific) for 1 h at room temperature. DAPI (Dojindo) nuclear staining was carried out thereafter, and the images were acquired using the DMI8 microscope with THUNDER imaging systems or the confocal microscope SP8 (Leica Microsystems).

The ALB status (i.e., low or high) of E11.5 liver was defined using the stained sections. After acquisition of auto color-scaled images in LAS X (Leica Microsystems), the background was subtracted using the color balance function on Fiji and minimum values of 0–40. ALB^{low} and ALB^{high} were defined as lower (i.e., <20) and higher (i.e., >20) mean gray values in a 400 μ m² area (2 μ m \times 20 μ m), respectively.

Single cell RNAseq analysis

The current study analyzed single-cell RNA-seq datasets downloaded from the CNGB Nucleotide Sequence Archive of CNGBdb and the NCBI Gene Expression Omnibus (accession numbers: GSE87038 and CNP0000236). The GSE87038 datasets were curated to focus on liver tissue samples and fetal times of E9.5, E10.5, and E11.5 using R (Fig. S6). Further data analyzes (i.e., filtering, normalization, dimensionality reduction, clustering, and visualization) were carried out using Seurat (version 4.1.1), and cell identification was performed using ScType on the CNP0000236 dataset. Publicly available datasets were analyzed^{3,51–53}.

RNA sequencing (RNAseq)

RNA quality checks were performed using the 4150/4200 RNA screen tape (Agilent tech, Santa Clara, California) kit, and 5 μ l of RNA sample buffer and 1 μ l of RNA sample was added to each vial. Vortex homogenization was performed for one minute, followed by incubation at 72 °C for 3 min. The samples were then moved to the icebox for 2 min. RNA integrity was evaluated using Agilent 4200 tapestation (Agilent Technologies, Santa Clara, California), and RNA samples with RNA integrity number >8.8 were subjected to RNA-Seq analysis. RNA-seq

libraries were prepared using 30 ng of total RNA using an Ion AmpliSeq Transcriptome Human Gene Expression kit according to manufacturer's instructions (Thermo Fisher Scientific, Waltham, MA). The libraries were sequenced with 100-bp single-end reads to a depth of at least 10 million reads per sample on the Ion Proton platform using an Ion PI Hi-Q Sequencing 200 kit and Ion PI Chip v3 (Thermo Fisher Scientific). Primary analysis of RNA sequencing data was performed using AmpliSeqRNA plug-in (v5.2.0.3), a Torrent Suite Software (v5.2.2, Thermo Fisher Scientific). Briefly, the sequence reads were aligned to hg19_AmpliSeq_Transcriptome_ERCC_v1 using the Torrent Mapping Alignment Program (TMAP). Raw counts and normalized reads per gene (RPM, reads assigned per million mapped reads) were generated, which were used for subsequent analysis. The data for IPA were extracted using the Subio platform (Subio, Kasugai, Japan). Our data is deposited in Gene Expression Omnibus (GEO) under accession code "GSE249213".

In silico analysis using ingenuity pathway analysis (IPA)

The Core analysis function of the IPA software (TOMY DIGITAL BIOLOGY) was used to extract important signaling pathways in the HEs, ECs, and MCs of hiPSC-liver organoids 7 days after IL1 α treatment. The datasets contained the fold change (IL1 α /control) and p-values from the RNA-seq data, and overlapping networks of HE, EC, and MC in the organoids were extracted.

ELISA

Placenta (1 tissue/well), heart (3 tissues/well), liver with STM (3 tissues/well), and fetus are cultured with Opti-MEM (serum-free, 1% penicillin-streptomycin) for 3 h. The supernatant was collected, and IL1 α concentration was measured in undiluted supernatant by Mouse IL-1 α ELISA Kit (ab199076) according to manufacturer's instructions.

The supernatant was collected in SAA1-treated hiPSC-liver organoid at day 7. CCL20 concentration was measured using the supernatant by Human MIP-3 alpha ELISA Kit (CCL20) (ab269562) according to manufacturer's instructions.

Statistics and reproducibility

All statistical analyzes were performed using GraphPad Prism 8.4 (GraphPad Software, Inc., CA, USA). The statistical tests used have been described in the figure legends. We confirmed the reproducibility by 2 or 3 independent experiments in each data.

Reporting summary

Further information on research design is available in the Nature Portfolio Reporting Summary linked to this article.

Data availability

Our RNAseq were deposited in NCBI GEO database under accession code (GSE249213). Mouse liver and placenta data generated in this study have been deposited in the NCBI GEO database under accession code GSE106465 and GSE100053. Mouse liver single cell data have been deposited in the NCBI GEO database under accession code GSE87038 and CNP0000236. Source data are provided with this paper.

References

- Takebe, T. et al. Vascularized and complex organ buds from diverse tissues via mesenchymal cell-driven condensation. *Cell Stem Cell* **16**, 556–565 (2015).
- Takebe, T. et al. Vascularized and functional human liver from an iPSC-derived organ bud transplant. *Nature* **499**, 481–484 (2013).
- Camp, J. G. et al. Multilineage communication regulates human liver bud development from pluripotency. *Nature* **546**, 533–538 (2017).
- Amabile, G. & Meissner, A. Induced pluripotent stem cells: current progress and potential for regenerative medicine. *Trends Mol. Med.* **15**, 59–68 (2009).
- Yamanaka, S. Pluripotent stem cell-based cell therapy—promise and challenges. *Cell Stem Cell* **27**, 523–531 (2020).
- Willnow, D. et al. Quantitative lineage analysis identifies a hepatopancreato-biliary progenitor niche. *Nature* **597**, 87–91 (2021).
- Wong, Y. F. et al. Expansion of ventral foregut is linked to changes in the enhancer landscape for organ-specific differentiation. *Nat. Cell Biol.* (2023) <https://doi.org/10.1038/s41556-022-01075-8>.
- Pu, W. et al. Bipotent transitional liver progenitor cells contribute to liver regeneration. *Nat. Genet.* **55**, 651–664 (2023).
- Wang, D. et al. Long-term expansion of pancreatic islet organoids from resident procr+ progenitors. *Cell* **180**, 1198–1211.e19 (2020).
- Tarlow, B. D. et al. Bipotential adult liver progenitors are derived from chronically injured mature hepatocytes. *Cell Stem Cell* **15**, 605–618 (2014).
- Medvinsky, A., Rybtsov, S. & Taoudi, S. Embryonic origin of the adult hematopoietic system: advances and questions. *Development* **138**, 1017–1031 (2011).
- Han, V. K. M., Seferovic, M. D., Albion, C. D. & Gupta, M. B. Intrauterine Growth Restriction: Intervention Strategies. in *Neonatology* 89–93 (Springer Milan, Milano, 2012). https://doi.org/10.1007/978-88-470-1405-3_13.
- Hyatt, M. A., Budge, H. & Symonds, M. E. Early developmental influences on hepatic organogenesis. *Organogenesis* **4**, 170–175 (2008).
- Mohan, R., Baumann, D. & Alejandro, E. U. Fetal undernutrition, placental insufficiency, and pancreatic β -cell development programming in utero. *Am. J. Physiol. Regul. Integr. Comp. Physiol.* **315**, R867–R878 (2018).
- Radford, B. N. & Han, V. K. M. Offspring from maternal nutrient restriction in mice show variations in adult glucose metabolism similar to human fetal growth restriction. *J. Dev. Orig. Health Dis.* **10**, 469–478 (2019).
- Kusuyama, J. et al. Placental superoxide dismutase 3 mediates benefits of maternal exercise on offspring health. *Cell Metab.* **33**, 939–956.e8 (2021).
- Abuzzahab, M. J. et al. IGF-I receptor mutations resulting in intrauterine and postnatal growth retardation. *N. Engl. J. Med.* **349**, 2211–2222 (2003).
- Lopez-Tello, J. et al. Fetal manipulation of maternal metabolism is a critical function of the imprinted Igf2 gene. *Cell Metab.* **35**, 1195–1208.e6 (2023).
- Lorenz, L. et al. Mechanosensing by β 1 integrin induces angiocrine signals for liver growth and survival. *Nature* **562**, 128–132 (2018).
- Tadokoro, T. et al. Human iPSC-liver organoid transplantation reduces fibrosis through immunomodulation. *Sci. Transl. Med.* **16**, eadg0338 (2024).
- Ream, M., Ray, A. M., Chandra, R. & Chikaraishi, D. M. Early fetal hypoxia leads to growth restriction and myocardial thinning. *Am. J. Physiol. Regul. Integr. Comp. Physiol.* **295**, 583–595 (2008).
- Takebe, T. et al. Massive and reproducible production of liver buds entirely from human pluripotent stem cells. *Cell Rep.* **21**, 2661–2670 (2017).
- Soncin, F. et al. Comparative analysis of mouse and human placentae across gestation reveals species-specific regulators of placental development. *Development* **145**, dev156273 (2018).
- Matsumoto, K., Miki, R., Nakayama, M., Tatsumi, N. & Yokouchi, Y. Wnt9a secreted from the walls of hepatic sinusoids is essential for morphogenesis, proliferation, and glycogen accumulation of chick hepatic epithelium. *Dev. Biol.* **319**, 234–247 (2008).
- Duncan, S. A. & Watt, A. J. BMPs on the road to hepatogenesis. *Genes Dev.* **15**, 1879–1884 (2001).

26. Jung, J., Zheng, M., Goldfarb, M. & Zaret, K. S. Initiation of mammalian liver development from endoderm by fibroblast growth factors. *Science* **284**, 1998–2003 (1999).
27. Deutsch, G., Jung, J., Zheng, M., Lora, J. & Zaret, K. S. A bipotential precursor population for pancreas and liver within the embryonic endoderm. *Development* **128**, 871–881 (2001).
28. Ayabe, H. et al. Optimal hypoxia regulates human iPSC-derived liver bud differentiation through intercellular TGFB signaling. *Stem Cell Rep.* **11**, 306–316 (2018).
29. Godet, I. et al. Fate-mapping post-hypoxic tumor cells reveals a ROS-resistant phenotype that promotes metastasis. *Nat. Commun.* **10**, 4862 (2019).
30. Kakni, P. et al. Hypoxia-tolerant apical-out intestinal organoids to model host-microbiome interactions. *J. Tissue Eng.* **14**, 20417314221149208 (2023).
31. Chen, A. et al. Spatiotemporal transcriptomic atlas of mouse organogenesis using DNA nanoball-patterned arrays. *Cell* **185**, 1777–1792.e21 (2022).
32. Ogawa, M. et al. Directed differentiation of cholangiocytes from human pluripotent stem cells. *Nat. Biotechnol.* **33**, 853–861 (2015).
33. Hagihara, K. et al. IL-6 plays a critical role in the synergistic induction of human serum amyloid A (SAA) gene when stimulated with proinflammatory cytokines as analyzed with an SAA isoform real-time quantitative RT-PCR assay system. *Biochem. Biophys. Res. Commun.* **314**, 363–369 (2004).
34. Sandri, S. et al. Serum amyloid A induces CCL20 secretion in mononuclear cells through MAPK (p38 and ERK1/2) signaling pathways. *Immunol. Lett.* **121**, 22–26 (2008).
35. Yamaguchi, T. et al. Interspecies organogenesis generates autologous functional islets. *Nature* **542**, 191–196 (2017).
36. Swartley, O. M., Foley, J. F., Livingston, D. P., Cullen, J. M. & Elmore, S. A. Histology atlas of the developing mouse hepatobiliary hemolymphatic vascular system with emphasis on embryonic days 11.5–18.5 and early postnatal development. *Toxicol. Pathol.* **44**, 705–725 (2016).
37. Kozak, K. R., Abbott, B. & Hankinson, O. ARNT-deficient mice and placental differentiation. *Dev. Biol.* **191**, 297–305 (1997).
38. Glaccum, M. B. et al. Phenotypic and functional characterization of mice that lack the type I receptor for IL-1. *J. Immunol.* **159**, 3364–3371 (1997).
39. Cullinan, E. B. et al. IL-1 receptor accessory protein is an essential component of the IL-1 receptor. *J. Immunol.* **161**, 5614–5620 (1998).
40. Tan, J. et al. CCL20/CCR6 axis mediates macrophages to promote proliferation and migration of ESCs by blocking autophagic flux in endometriosis. *Stem Cell Res. Ther.* **13**, 294 (2022).
41. Matsumoto, K., Yoshitomi, H., Rossant, J. & Zaret, K. S. Liver organogenesis promoted by endothelial cells prior to vascular function. *Science* **294**, 559–563 (2001).
42. Lammert, E., Cleaver, O. & Melton, D. Induction of pancreatic differentiation by signals from blood vessels. *Science* **294**, 564–567 (2001).
43. Minato, T. et al. Relationship between short term variability (STV) and onset of cerebral hemorrhage at ischemia-reperfusion load in fetal growth restricted (FGR) mice. *Front. Physiol.* **9**, 1–11 (2018).
44. Xiong, S. et al. Interleukin-1RA mitigates SARS-CoV-2-Induced inflammatory lung vascular leakage and mortality in humanized K18-hACE-2 mice. *Arterioscler. Thromb. Vasc. Biol.* **41**, 2773–2785 (2021).
45. Takebe, T. et al. Generation of a vascularized and functional human liver from an iPSC-derived organ bud transplant. *Nat. Protoc.* **9**, 396–409 (2014).
46. Krumm, J. et al. High temporal resolution proteome and phosphoproteome profiling of stem cell-derived hepatocyte development. *Cell Rep.* **38**, 110604 (2022).
47. Matsui, S. et al. Characterization of peribiliary gland-constituting cells based on differential expression of trophoblast cell surface protein 2 in biliary tract. *Am. J. Pathol.* **188**, 2059–2073 (2018).
48. Padmanaban, V. et al. Organotypic culture assays for murine and human primary and metastatic-site tumors. *Nat. Protoc.* **15**, 2413–2442 (2020).
49. Zhao, S. et al. Cellular and molecular probing of intact human organs. *Cell* **180**, 796–812.e19 (2020).
50. Yokomizo, T. et al. Whole-mount three-dimensional imaging of internally localized immunostained cells within mouse embryos. *Nat. Protoc.* **7**, 421–423 (2012).
51. Mu, T. et al. Embryonic liver developmental trajectory revealed by single-cell RNA sequencing in the Foxa2eGFP mouse. *Commun. Biol.* **3**, 642 (2020).
52. Dong, J. et al. Single-cell RNA-seq analysis unveils a prevalent epithelial/mesenchymal hybrid state during mouse organogenesis. *Genome Biol.* **19**, 1–20 (2018).
53. Ianevski, A., Giri, A. K. & Aittokallio, T. Fully-automated and ultra-fast cell-type identification using specific marker combinations from single-cell transcriptomic data. *Nat. Commun.* **13**, 1–10 (2022).

Acknowledgements

We would like to thank all team members for providing technical support and the FACS core laboratory IMSUT for kindly assisting with cell sorting. This work was supported by the Japan Agency for Medical Research and Development AMED; JP13bm0304002, JP20bk0104102h0001, JP21fk0210073s0502, JP23fk0210129s0501, JP23bm1223007, JP24bk0104174h0001 to H.T. and the Ministry of Education, Culture, Sports, Science, and Technology (MEXT; 21H04830, 24H00641 to H.T.; 19K18034, 22K16440 to Y.K.). We would also like to thank Enago (www.enago.jp) for reviewing the language of the manuscript.

Author contributions

Y.K. and N.T.: study conception and design; Y.K., N.T., and H.T.: preparation of manuscript; Y.K., S.M., S.T., E.C., T. Okumura, S.Y., T.K., K.Y., Y.F., and T. Oba: performed experiments; T.T., Y.U., and T. Oba: provided intellectual support; Y.K. and H.T.: acquired funding. All authors have read and agreed to the final version of the manuscript prior to submission.

Competing interests

The authors declare no competing interests.

Additional information

Supplementary information The online version contains supplementary material available at <https://doi.org/10.1038/s41467-025-57551-w>.

Correspondence and requests for materials should be addressed to Hideki Taniguchi.

Peer review information *Nature Communications* thanks Kimberly D. Tremblay, Meritxell Huch, and the other anonymous reviewer for their contribution to the peer review of this work. A peer review file is available.

Reprints and permissions information is available at <http://www.nature.com/reprints>

Publisher's note Springer Nature remains neutral with regard to jurisdictional claims in published maps and institutional affiliations.

Open Access This article is licensed under a Creative Commons Attribution-NonCommercial-NoDerivatives 4.0 International License, which permits any non-commercial use, sharing, distribution and reproduction in any medium or format, as long as you give appropriate credit to the original author(s) and the source, provide a link to the Creative Commons licence, and indicate if you modified the licensed material. You do not have permission under this licence to share adapted material derived from this article or parts of it. The images or other third party material in this article are included in the article's Creative Commons licence, unless indicated otherwise in a credit line to the material. If material is not included in the article's Creative Commons licence and your intended use is not permitted by statutory regulation or exceeds the permitted use, you will need to obtain permission directly from the copyright holder. To view a copy of this licence, visit <http://creativecommons.org/licenses/by-nc-nd/4.0/>.

© The Author(s) 2025